Effects of artificial barriers on the propagation of debris avalanches

Sabatino Cuomo*, Sabrina Moretti^, Stefano Aversa^

* GEG, Geotechnical Engineering Group, University of Salerno
Via Giovanni Paolo II, 132, 84084 Fisciano (Salerno), Italy
^ Dept. of Engineering, University of Naples "Parthenope"
Centro Direzionale, Isola C4, 80133 Napoli, Italy

ABSTRACT

The paper deals with the effects of artificial barriers on the dynamic features of unconfined flows such as debris avalanches in coarse-grained materials. These phenomena are often responsible for damage to structures and risk to human life. Artificial barriers could mitigate those threats by reducing the flow velocity and the runout distance as well as diverting the flow towards lateral zones constrained by the barriers. A quasi-3D SPH hydro-mechanically coupled model was used to simulate the propagation heights and velocities, the evolution of pore water pressures inside the flow and the entrainment of additional material from the ground surface during the propagation stage. The numerical simulations referred to: i) simple topography resembling typical in-situ conditions; ii) the case history of Nocera Inferiore (Southern Italy) where a destructive debris avalanche occurred in 2005. Different scenarios were analysed relative to the number, type and location of the artificial barriers. The numerical results highlight the variations in propagation pattern, velocity, and deposition thickness of the flows, which may occur in presence of artificial barriers. Indications on favourable type and location of barriers are provided both for the simple topography and for the specific case study.

Keywords: SPH, propagation, barrier, debris avalanche, flow

1 INTRODUCTION

Unconfined flows comprise a large series of natural processes including rock avalanches, pyroclastic flows, and debris avalanches, which propagate along the slopes far from drainage lines, ravines, or valleys. They are extremely rapid, travel hundreds of metres, and increase in volume during the propagation stage (Cascini et al., 2014). Flows in fine-grained materials are generally elongated (Hurlimann et al., 2015), while those occurring in coarse-grained materials may have a significant lateral spreading (Cascini et al., 2016). The latter is typical for a "debris avalanche", which Hungr et al. (2001, 2014) define as a "very rapid to extremely rapid shallow flow of partially or fully saturated debris on a steep slope, without confinement in an established channel". The scientific literature clearly evidences that debris avalanches have a minor mobility compared to other flows

(Cascini et al., 2011a). This relates to the faster dissipation of the pore water pressures compared to the case of channelised flows. In fact, most debris avalanches stop at the toe of the slope.

Previous propagation analyses of flow-type landslides have been proposed using a variety of methods (e.g. Finite Element Method, Finite Difference Method, Discrete Element Method), among which Smoothed Particle Hydrodynamics (SPH) provided a good compromise of accuracy and time efficiency (Pastor et al., 2009; Cuomo et al., 2014; Braun et al., 2018). Small-sized flume tests, real case histories and also the force (or pressure) of a flow impacting a barrier have been investigated so far. In this regard, analytical formulations for the impact explicitly consider: (h) height (Armanini et al., 2011); (v) velocity (Bugnion et al., 2011); both height and velocity (Ceccato et al., 2017; Canelli et al., 2012; Armanini et al., 2011); or combinations of the previous factors, such as the Froude number, defined as $v/(g \cdot h)^{0.5}$, being v the above mentioned flow velocity (Vagnon et al., 2016), or the compression waves velocity within the impacting medium (Calvetti et al., 2016).

In order to cope with the threat related to debris flows, rigid or flexible artificial barriers have been used in the field to modify height or velocity (Wendeler et al., 2007) or to stop the debris flow such as sabo dams (Mizuyama, 2008) and check dams (Popescu et al., 2009). Numerical analyses demonstrate that the obstacles appropriately reduce the runout distance and velocity of the flow-like landslides (Cuomo et al., 2017; Gioffrè et al., 2018). In other cases, the baffles reduced the peak dynamic impact forces of the flow (Choi et al., 2015b). For instance, Ng et al. (2015) analysed the interaction between baffles and debris flows through flume model experiments. Kwan et al. (2015) studied the effect of a series of barriers on landslides using numerical analyses and flume scale tests, disregarding the 3D effects. The role of geometry and number of obstacles has been recently analysed (Kattel et al., 2018). However, the literature still lacks contributions about the effectiveness of artificial barriers located at different positions in the piedmont zone and considering different features of the flow. Neither the efficiency of such barriers has been analysed in relation to the features of flows nor a consolidated design strategy is available for check dams or barriers subject to horizontal forces.

In this paper, debris avalanches are analysed focusing on flow features, such as height and velocity, and deposition area along simplified or real 3D topographies. Novel numerical analyses are proposed relative to: i) simple topography resembling typical in-situ conditions (Cuomo et al., 2014) and ii) the case history of Nocera Inferiore (Southern Italy), where a destructive debris avalanche occurred in 2005 (Cascini et al., 2016). Different scenarios are analysed for different numbers, types and locations of the artificial barriers. For all cases, the runout and the features of the flow are computed providing insights on the feasibility and efficiency of barriers used to protect the piedmont area.

2 MATERIALS AND METHODS

A barrier installed in the piedmont zone should be capable to resist to the dynamic actions exerted by the impacting flow, while its deformation and displacement are small enough to not significantly change the geometry of the barrier during the flow propagation. In such a process, three scenarios may occur: i) the flow stops behind the barrier; ii) the flow overtops the barrier but its velocity (and possibly, height) is reduced; iii) the barrier is badly located and the propagation features of the flow are not changed to acceptable values. A sketch of the three scenarios is provided in Fig. 1. Behind the barrier, in any of the three scenarios, the flow velocity reaches a peak value and then decreases to zero as the material stops. In the same time lapse, the landslide height increases up to the deposition thickness. At this location, the Froude number may greatly change in time, and this issue will be investigated in this paper. Specifically, the time interval between the arrival and the deposition of the flowing material behind the barrier will be referred to as "impact stage".

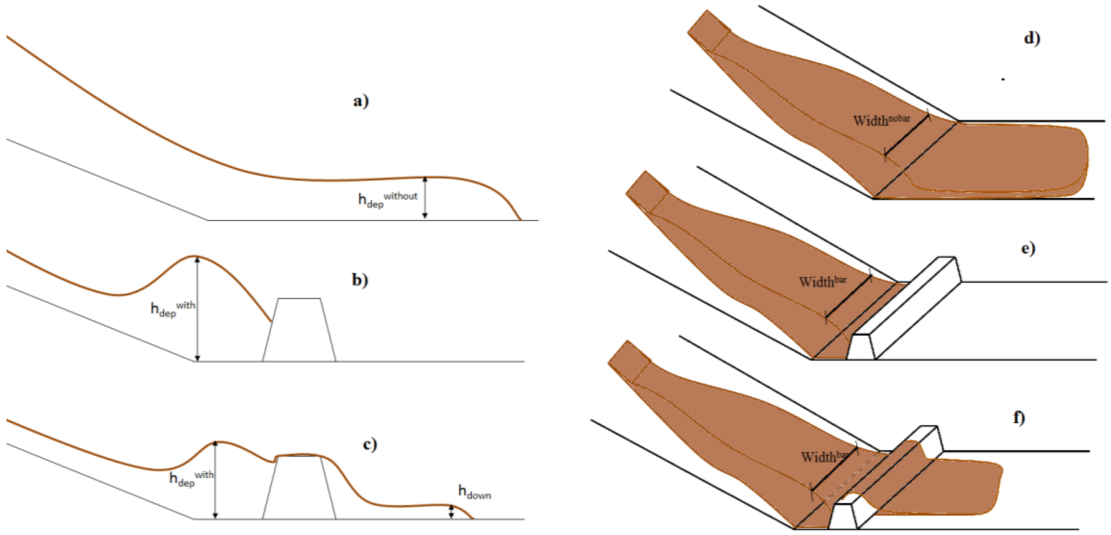

Figure 1. Different scenarios of flow propagation: a, d) natural slope; b, e) slope engineered with a barrier capable to stop the flow; c, f) flow overcoming the barrier.

The "GeoFlow_SPH" model, which is herein used, schematises the propagating mass into a mixture of a solid skeleton and pore water. It is a continuum-based approach based on a set of partial differential equations such as: i) the balance of mass of the mixture combined to the balance of the linear momentum of the pore fluid; ii) the balance of the linear momentum of the mixture; iii) the rheological equation of the mixture; iv) the kinematical relations between velocity and deformation. It is a quasi-3D model, as the fundamental equations are depth-integrated. The framework of Smoothed Particle Hydrodynamics (SPH) numerical method is used. The flowing mass is subdivided into a cluster of computational points, each of them moving along the topographic surface and transporting part of the landslide mass for which information about height, velocity, pore water pressure and bed erosion are computed in time. The mathematical and numerical details of the model are provided in Pastor et al. (2009) and Cuomo et al. (2014).

The main mechanisms included in the model are: i) the pore water pressure dissipation in the flowing material due to consolidation along the normal direction to the ground surface (Cascini et al., 2014) and ii) the entrainment of bed material along the propagation path (Cuomo et al., 2014). For the latter issue, we considered the entrainment rate (e_r) as $e_r = K\,h\,v\,(\tan\theta)^{2.5}$, where K is an empirical parameter that can be back-calculated from analysis of past events, θ is the local slope angle, *h* is the flow height and v is the flow velocity (Blanc, 2008). Another important factor in the flow propagation is the rheology of the flowing material (Cascini et al., 2016; Cuomo et al., 2016).

The input data used for the numerical modelling were: the Digital Terrain Model (DTM) of the simplified topography or real study areas, the rheological features of the flow, and the geometry, number and relative position of the barriers. The frictional rheological model is regarded as reliable for flows involving saturated granular materials (Pastor et al., 2014) and the rheological parameters are taken from the literature as listed below. Two geometries (trapezoid or compound cross section) of the barriers were investigated.

In this paper, the barriers are simply considered as geometrical modifications of the ground surface and they are assumed as not erodible by the flow. In the case of two barriers, they are still not erodible, while the zone between them can be eroded. The position and the geometry of the barrier are assumed as fixed during the impact stage. These assumptions rely on the fact that the local displacements in a well-designed barrier should be limited to some centimetres. The evaluation of the flow energy dissipation due to the impact against the barrier is beyond the scope of this work and is not included in the numerical analyses. This means that the simulated values of flow height and flow velocity must be considered as a safe overestimation of the real values.

We calculated the Froude number of the flow from the computed height and velocity at reference points behind the barriers. $Fr > 1$ corresponds to a supercritical flow, whose propagation is independent on the conditions along the flow path. The flow is subcritical for $Fr < 1$, i.e. influenced by downstream conditions (Choi et al., 2015; Cascini et al., 2018). Based on current literature, supercritical flows usually result in a vertical jet mechanism impacting a rigid barrier (i.e. the flow develops upwards even along vertical walls); whereas subcritical flows may show a mild reflective wave mechanism (Choi et al., 2015).

Two parameters are newly proposed for the flow propagation analysis, namely the Index of Piedmont Runout Reduction (I_{PRR}) and the Index of Lateral Spreading (I_{LS}), which read as:

$$I_{PRR} = \frac{PR_{eng}}{PR_{nat}} \tag{1}$$

$$I_{LS} = \frac{W_{eng}}{W_{nat}} \tag{2}$$

where PR_{eng} is the Piedmont Runout distance travelled by the flow inside the piedmont zone engineered with barriers, PR_{nat} is the runout inside the piedmont zone for the natural slope, W_{eng} is the maximum lateral width of the flow behind the barrier for the engineered slope, and W_{nat} is the analogous feature of the flow computed at the same point for the natural slope.

An I_{PRR} < 1.0 is desirable, and the lower I_{PRR}, the better the efficiency of the barrier. I_{PRR} also depends on where the barriers are located. A barrier favours the flow material to spread laterally and it is expected that I_{LS} > 1.0. For multiple barriers, I_{LS} is computed with the highest W_{eng} obtained for each barrier.

In addition, the Relative Pore Water Pressure (RPWP) is defined as the ratio between the water pressure and the total vertical pressure of the flow (Cascini et al., 2016), and it is computed in the time-space domain throughout the propagation-deposition process.

3 ANALYSIS OF SIMPLE TOPOGRAPHY CASE

3.1 Input data

A schematic open slope is firstly analysed, which is composed of two differently inclined planes and a debris avalanche triggered at the uppermost portion of the slope. The computational scheme and the soil properties are taken from Cuomo et al. (2014), who extensively investigated the role of the several factors involved in the propagation stage of a debris avalanche.

The slopes are inclined with 30° or 40° with different lengths (horizontal projection) L_1 (Fig. 2a). The piedmont zone is flat or gently inclined (10° steep) with length L_2. The length and the width of the source area are L_{trig} and B_{trig}, respectively, and H_{trig} is the initial height of soil inside the source area. A selection of the several numerical simulations performed are reported in Table 1, with L_1=230 m, L_2=500 m, the width of the slope (B) equal to 800 m, and the slope height (H_{slope}) equal to 222 m or 130 m for α_P=10° or α_P=0°, respectively .The DTM cell size is equal to 1.1 m for both slopes, inclined with 40° and 30°.

One or more barriers are added in the piedmont zone (Fig. 2). Each barrier is 5 m high (H), with top width (b) equal to 3 m, the upslope raceway (a) 3 m wide, and both lateral fronts inclined with 60° (Fig. 2b). The Type I barrier has a trapezoidal shape; the Type II barrier is similar but with an additional step (H/2 high, and large as b) located upslope. In the simulations, the first barrier is in the piedmont zone, specifically 10 m (x=240 m) or 25 m (x = 255 m) or 50 m (x = 280 m) downslope the divide between the slope and the piedmont.

Different sets of soil properties, such as the soil unit weight (γ), the friction angle (tanφ), the initial height of water table divided by the soil thickness (h_{wrel}), the initial value of relative pore water pressure (RPWP), the dimensions of the source area (L_{trig}, B_{trig}) and the initial height of the flow (h_{trig}) are taken from Cuomo et al. (2014), resembling the features of catastrophic events that occurred in Southern Italy, such as those of Cervinara in 1999 (Cascini et al., 2011b), and Nocera Inferiore in 2005 (Cuomo et al., 2014). Therefore, this paper extends the previous literature to the cases of a debris avalanche mitigated by barriers located in the piedmont zone.

The number of computational points is equal to 484,120, initially spaced 1.1 m for the slope inclined with 40°, while the number of computational points is equal to 80,758, initially spaced 1.1 m for the slope inclined with 30°. The time step of the numerical analyses is set to 0.5 s. For both types of barriers we defined a control point (P) behind the barrier to monitor in time the computed height and velocity of the flow (Fig. 2a-b).

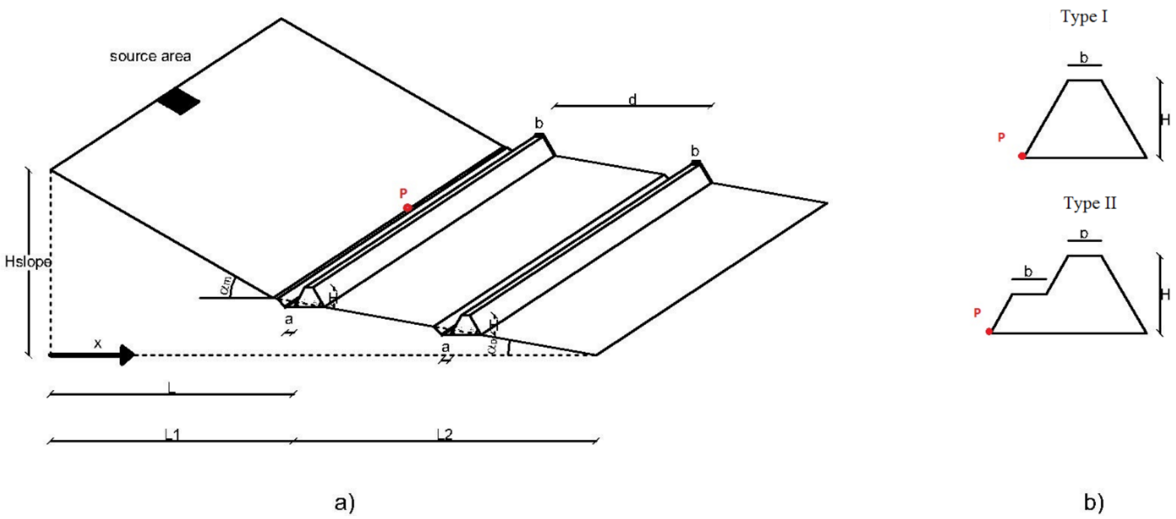

Figure 2. Simple topography (a) and types of barriers (b) considered in the numerical analyses.

Table 1. List of selected numerical cases for the slope inclined with 40°.

Case	α_p (°)	B_{trig} (m)	L_{trig} (m)	h_{trig} (m)	tanφ (-)	h_w^{rel} (m)	RPWP (-)	Type of barrier	L (m)
S1	10	50	100	1.0	0.52	0.40	0.5	none	-
S2	10	50	100	1.0	0.52	0.40	0.5	I	245
S3	10	50	100	1.0	0.52	0.40	0.5	II	245
S4	10	50	100	1.0	0.52	0.40	0.5	I	255
S5	10	50	100	1.0	0.52	0.40	0.5	II	255
S6	10	50	100	1.0	0.52	0.40	0.5	I	280
S7	10	50	100	1.0	0.52	0.40	0.5	II	280
S8	10	50	100	1.0	0.52	0.40	0.5	I	245-255
S9	10	10	26	4.0	0.30	0.75	1.0	none	-
S10	10	10	26	4.0	0.30	0.75	1.0	I	245
S11	10	10	26	4.0	0.30	0.75	1.0	II	245
S12	10	10	26	4.0	0.30	0.75	1.0	I	255
S13	10	10	26	4.0	0.30	0.75	1.0	II	255

S14	10	10	26	4.0	0.30	0.75	1.0	I	280
S15	10	10	26	4.0	0.30	0.75	1.0	II	280
S16	10	10	26	4.0	0.30	0.75	1.0	II	245-255
S17	10	10	26	4.0	0.30	0.75	1.0	II	255-280
R1	0	50	100	1.0	0.52	0.40	0.5	none	-
R2	0	50	100	1.0	0.52	0.40	0.5	I	245
R3	0	50	100	1.0	0.52	0.40	0.5	II	245
R4	0	50	100	1.0	0.52	0.40	0.5	I	255
R5	0	50	100	1.0	0.52	0.40	0.5	II	255
R6	0	50	100	1.0	0.52	0.40	0.5	I	245-255
R7	0	10	26	4.0	0.30	0.75	1.0	none	-
R8	0	10	26	4.0	0.30	0.75	1.0	I	245
R9	0	10	26	4.0	0.30	0.75	1.0	II	245
R10	0	10	26	4.0	0.30	0.75	1.0	I	255
R11	0	10	26	4.0	0.30	0.75	1.0	II	255
R12	0	10	26	4.0	0.30	0.75	1.0	I	280
R13	0	10	26	4.0	0.30	0.75	1.0	II	280
R14	0	10	26	4.0	0.30	0.75	1.0	I	245-255
R15	0	10	26	4.0	0.30	0.75	1.0	I	255-280

α_p: slope angle of piedmont area; L_{trig}: length of landslide source area; B_{trig}: width of landslide source area; h_{trig}: initial height of trigger area; $tan\ \varphi$: friction angle; h_w^{rel}: relative water height; *RPWP*: relative pore water pressure; *L*: distance between the barrier and source area.

Table 2. List of the numerical cases selected for the 30° steep slope.

Case	α_p (°)	B_{trig} (m)	L_{trig} (m)	h_{trig} (m)	tanφ (-)	h_w^{rel} (m)	RPWP (-)	Type of barrier	*L* (m)
S18	10	50	100	1.0	0.52	0.40	0.5	none	-
S19	10	50	100	1.0	0.52	0.40	0.5	I	245
S20	10	50	100	1.0	0.52	0.40	0.5	II	245
S21	10	50	100	1.0	0.52	0.40	0.5	I	255
S22	10	50	100	1.0	0.52	0.40	0.5	II	255
S23	10	50	100	1.0	0.52	0.40	0.5	I	280
S24	10	50	100	1.0	0.52	0.40	0.5	II	280

S25	10	10	26	4.0	0.30	0.75	1.0	none	-
S26	10	10	26	4.0	0.30	0.75	1.0	I	245
S27	10	10	26	4.0	0.30	0.75	1.0	II	245
S28	10	10	26	4.0	0.30	0.75	1.0	I	255
S29	10	10	26	4.0	0.30	0.75	1.0	II	255
S30	10	10	26	4.0	0.30	0.75	1.0	I	280
S31	10	10	26	4.0	0.30	0.75	1.0	II	280
S32	10	10	26	4.0	0.30	0.75	1.0	I	255-280
R16	0	50	100	1.0	0.52	0.40	0.5	none	-
R17	0	50	100	1.0	0.52	0.40	0.5	I	245
R18	0	50	100	1.0	0.52	0.40	0.5	II	245
R19	0	50	100	1.0	0.52	0.40	0.5	I	255
R20	0	50	100	1.0	0.52	0.40	0.5	II	255
R21	0	10	26	4.0	0.30	0.75	1.0	none	-
R22	0	10	26	4.0	0.30	0.75	1.0	I	245
R23	0	10	26	4.0	0.30	0.75	1.0	II	245
R24	0	10	26	4.0	0.30	0.75	1.0	I	255
R25	0	10	26	4.0	0.30	0.75	1.0	II	255
R26	0	10	26	4.0	0.30	0.75	1.0	I	245-255

α_p: slope angle of piedmont area; L_{trig}: length of landslide source area; B_{trig}: width of landslide source area; h_{trig}: initial height of trigger area; $\tan\varphi$: friction angle; h_w^{rel}: relative water height; *RPWP*: relative pore water pressure; *L*: distance between the barrier and source area..

3.2 Numerical results

Some of the simulated debris avalanches are shown in Figure 3 at the final time step. The barrier reduces the runout in the piedmont zone either if the barrier completely stops the flow (Cases S23, R24) or the barrier is overtopped (Cases S21, R22). The deposition zone and area affected by each simulated flow depend on the initial failure volume, rheology, type and position of the barrier(s). For the three largest simulated avalanches (initial volume of 5,000 m^3) propagating over a gentle or flat piedmont, the height of the landslide deposit increases by about 5 m with one barrier (cases S23, S21) compared to the natural slope (case S18). The flowing material overtops the barrier in Case S21, while it stops behind the barrier in Case S23. In both cases, the runout distance decreases by about 50 m with the presence of the barrier. The smaller avalanches (initial volume of about 260 m^3) have similar behaviour independent on the piedmont steepness. The runout decreases by a few meters due to the barrier (cases R24, R22 versus case R21) and the deposit thickness increases of about 1 m behind the barrier (Fig. 3). More in general, the height of the flows always increases behind the barrier (cases S21, S23, R22, R24) compared to the natural slope (cases S18, R21).

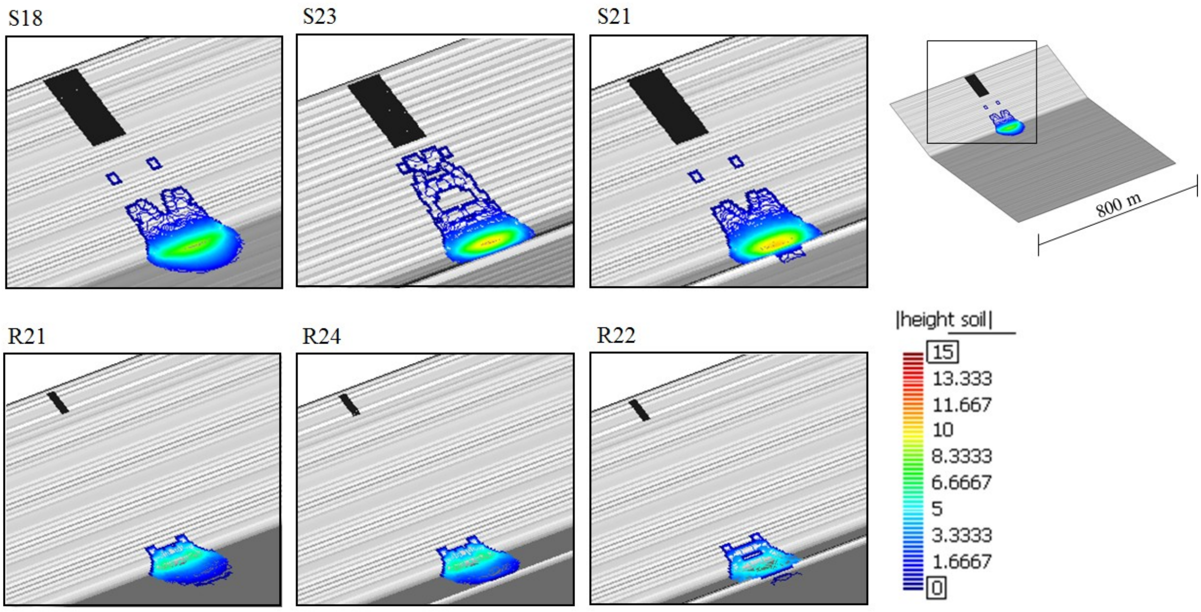

Figure 3. Flow deposits for different cases.

The change in time of the Froude number (*Fr*) was estimated at point P using the computed *h*-*v* pairs (Fig. 2). If $Fr < 1$, as the flow is subcritical, the barrier is expected to modify the flow propagation, while for $Fr >> 1$ the barrier would not perform well but still contribute to reducing the flow velocity. During the impact stage, the Froude number raises to 3.0 – 4.5 depending on flow rheology (Fig. 4a, b), and in most of the cases it is lower than for the natural slope (Case S1, and Case S9).

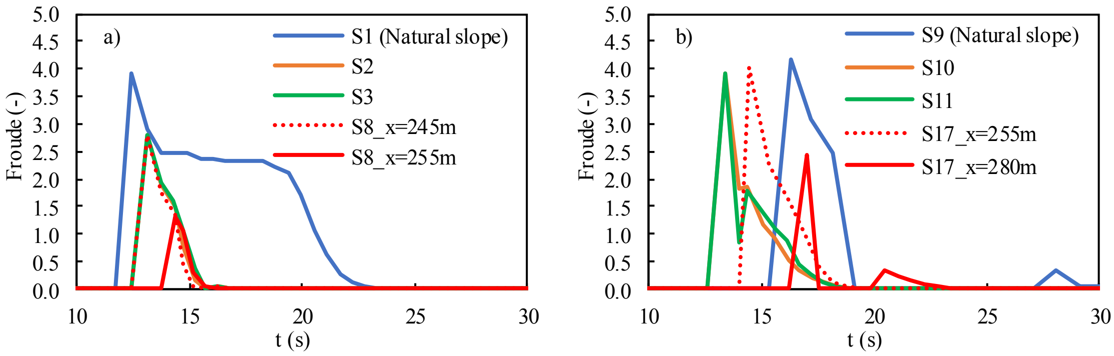

Figure 4. Time trend of Froude number computed at point P of figure 2b during the impact stage for: a) rheology 1; b) rheology 2.

The values of RPWP reported in Fig. 5 were calculated considering the maximum pore water pressures computed along the slope profile during the impact stage duration (typically a few seconds long, as shown in Fig 4). The presence of a barrier can cause PRWP to increase irrespective of the number of barriers and flow rheology (Fig. 5). For the Type I barrier, RPWP increases to 0.14 and 1.0 in Case S2 and Case S10, respectively. For the Type II barrier, RPWP reaches 0.13 and 0.98 (Case S3 and Case S11) while for two barriers RPWP is 0.12 and 0.85 (Case S8 and Case S17), respectively.

The presence of barriers reduced also the cumulative erosion thickness (h_{er}) along the slope for rheology 1 (Fig. 6a), while the reduction of erosion thickness was not appreciable for rheology 2 (Fig. 6b).

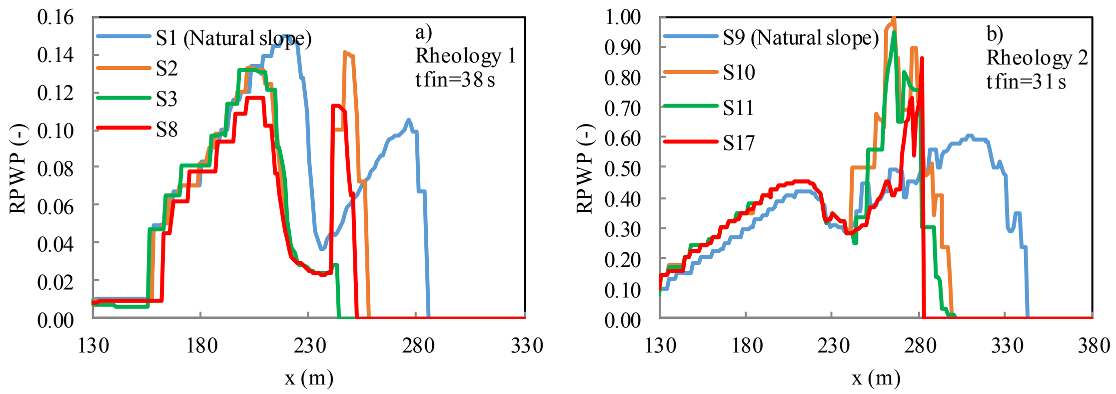

Figure 5. Envelope of pore water pressure along the slope during 20 seconds for: a) rheology 1, b) rheology 2.

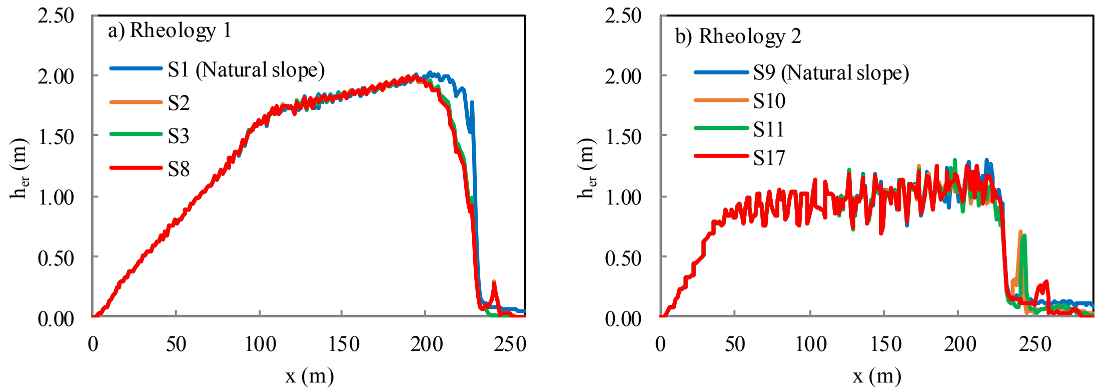

Figure 6. Cumulative erosion thickness along the slope at final step for: rheology 1 (a), rheology 2 (b).

The computed values of I_{PRR} and I_{LS} are reported in Fig. 7 for all cases. Four zones can be individuated in the plots: 1) I_{PRR}<1.0 and I_{LS}<1.0, i.e. both runout and width decrease, meaning that the barrier is effective. This is an unlikely condition; 2) I_{PRR}<1.0 and I_{LS}>1.0, i.e. the runout diminishes while the width increases, meaning the barrier is still effective. This is a very likely condition; 3) I_{PRR}>1.0 and I_{LS}>1.0, i.e. both runout and the width increase and thus the barrier is ineffective in terms of reduction of runout; 4) I_{PRR}>1.0 and I_{LS}<1.0, i.e. there is a reduction of width and an increase of runout, so that the barrier is ineffective. However, this condition is unrealistic. For two barriers, we considered the maximum width of flow in the plane-view. The computed runout is always reduced with one or two barriers, irrespective of overtopping. In general, runout can be reduced to 70% (Case S3) with a maximum increase of lateral spreading of 5% compared to the natural slope. Furthermore, the barrier type differently influences the area affected by the flow. In particular, I_{PRR} decreases, passing from Type I to Type II for the same position of the barriers (Case S4 and Case S5, or Case R17 and Case R18). The barrier type does not influence I_{PRR} for barriers located very far from the landslide source area (Cases S6 and S7, R24 and R25).

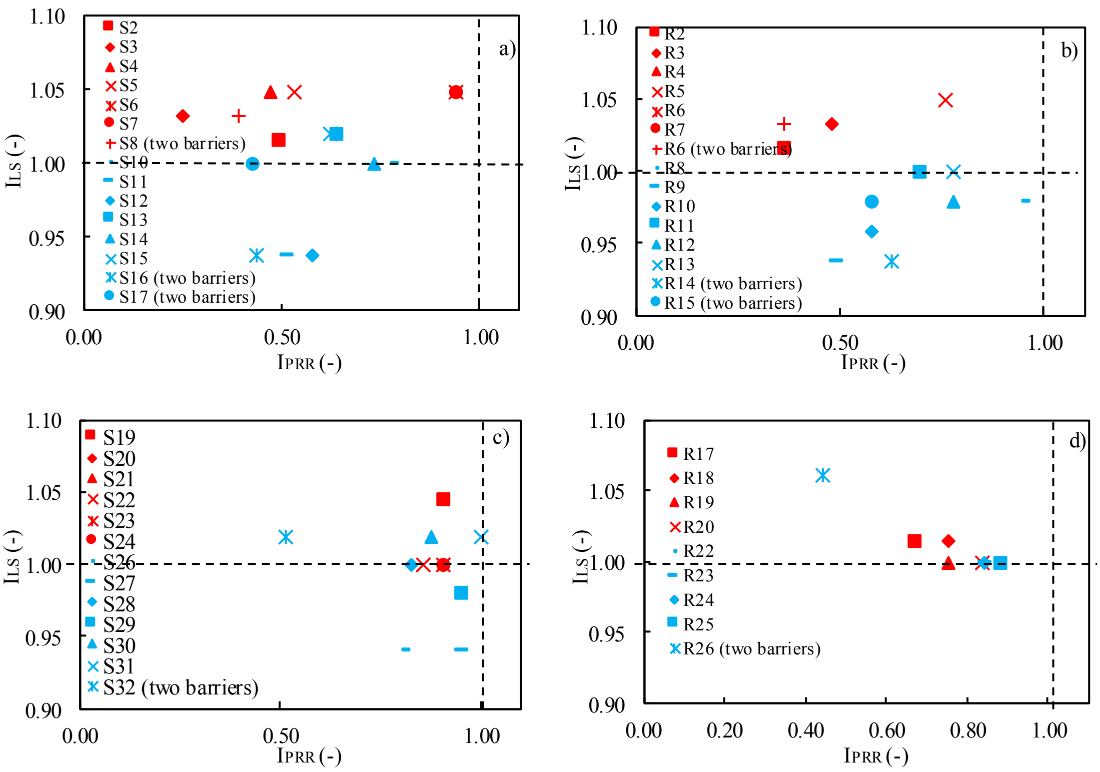

Figure 7. Indexes I_{PRR} and I_{LS} computed for different rheologies (R1: red; R2: blue) and different slopes: a), b) inclined with 40° (cases listed in Table 1); c), d) inclined with 30° (cases listed in Table 2).

4 Case study

4.1 Input data

The proposed methodology was applied to a site where a catastrophic debris avalanche occurred in 2005 (Fig. 11a). In the Monte Albino site (Nocera Inferiore, Italy) an open slope, on average 35° steep, is still susceptible to future debris avalanches and potential control works could consist of barriers installed at the piedmont area. In contrast to the previous simple topography case, the case study presents a channel along the slope where the flow could be channelized inside (Fig. 8b).

The DTM cell size is equal to 1.75 m, providing a satisfactory description of the site (Fig. 8b). We considered the two previous types (I, II) of the barriers (Fig. 2b) with 5 m or 7 m height (H), with a top width equal to 3 m (b), with the upslope raceway 3 m wide (a), and both lateral fronts inclined with 60° (Fig. 2b). The barriers are located at about 120 m a.s.l. following the local elevation contour lines. Various analyses are performed with different positions and types of the barriers. The control points (Q, T) are selected at the base of the upslope side of the barriers as shown in Fig. 8c-d.

The numerical simulations are listed in Table 3, with reference to the different features of the barrier (type, H, L). The rheological properties and the initial conditions of the flow material are taken from Cuomo et al. (2014), i.e. $\gamma = 13.0$ kN/m^3, $\tan\varphi = 0.4$, $h_w^{rel} = 0.25$, $p_w^{rel} = 1.0$. The soil is mobilized from the real source area observed in 2005 and the features is also taken from the literature ($A_{trig} = 2{,}369$ m^2 and $h_{trig} = 1.5$ m). The time step for the numerical analyses is set at 0.5 s.

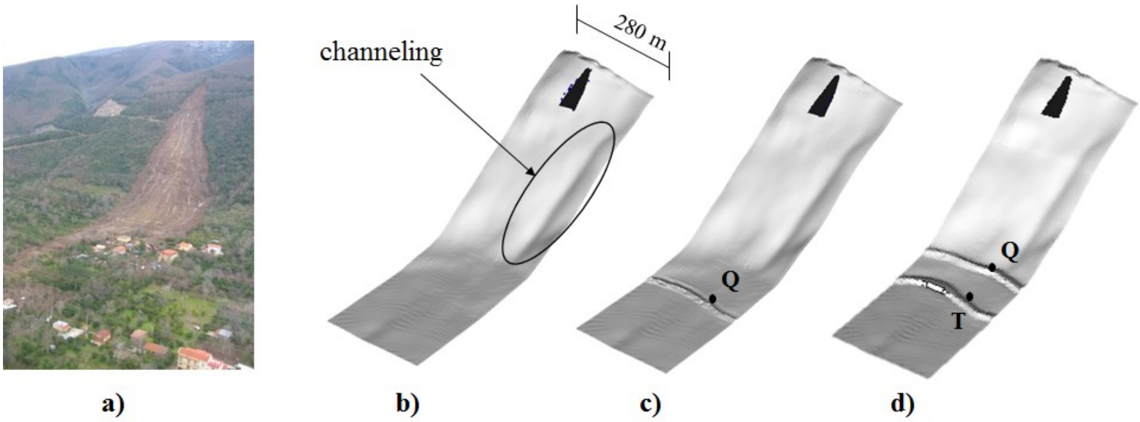

Figure 8. Case study: a) picture of 2005 debris avalanche (Cuomo et al., 2014); DTM and source area used for modelling the propagation along the natural slope (b); or along the slope engineered with one barrier (c) or two barriers (d).

Table 3. List of the selected numerical cases.

Case	type (-)	H (m)	L (m)	Case	type (-)	H (m)	L (m)
N1	None	-	-	*N10*	I	7	435
N2	I	7	575	*N11*	I	7	415
N3	I	5	575	*N12*	II	5	495
N4	II	5	575	*N13*	II	5	435
N5	II	5	435-575	*N14*	II	5	415
N6	I	5	495	*N15*	II	7	495
N7	I	5	435	*N16*	II	7	435
N8	I	5	415	*N17*	II	7	415
N9	I	7	495				

H: height of the barrier; *L*: distance of the barrier from the landslides source area.

4.2 Results

Some of the simulated debris avalanches are shown in Fig. 9 at the final time step for the natural slope (Case N1), an engineered slope with one non-overtopped barrier (Case. N3), a slope with one overtopped barrier (Case N6), and a slope with two barriers (Case N5). As expected, the final deposition zone and the whole area affected by each simulated flow depend on the type and position of the barriers. Similarly to the previous analyses of the simple topography slopes, the debris height at the control points behind the barriers increases compared to the case of the natural slope (Fig. 9). At the same time, the lateral spreading of flow increases behind the barrier, an effect that becomes clearer when the barrier is closer to the slope (e.g. Case N5).

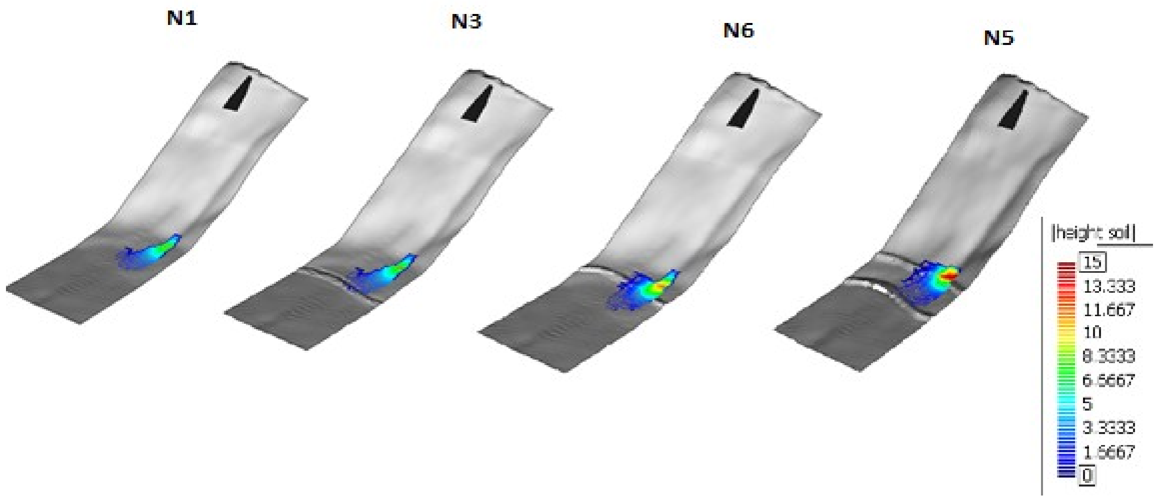

Figure 9. Soil deposit for different cases of barrier and slope design.

The time histories (or chronological changes) of the Froude number were calculated at point Q for different cases using the computed heights and velocities (Fig. 10). Froude numbers range from 2.0 to 3.0 for the cases of overtopped barriers irrespective of the distance from the source area (i.e. 415 m, 435 m, or 495 m). The peak values of the Froude number are 3.0 to 5.0 for the not-overtopped barriers. The height of the barrier has little effect on the Froude number (Case N2 and N3), while the peak of the Froude number for Type II (Case N4) is reached at around 25 s, several seconds earlier than those for Type I (Case N2). The Froude number is lower when barriers are present, whether they are overtopped or not.

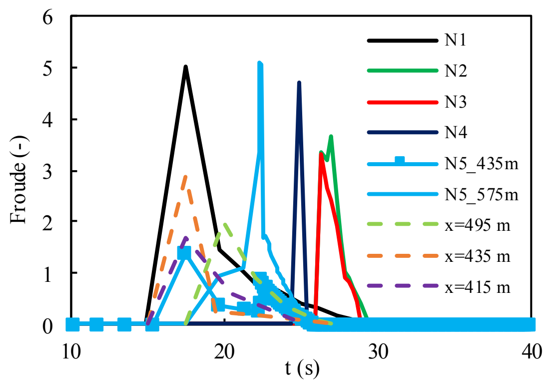

Figure 10. Time trend of Froude number computed at the control point (Q or T of figure 10) during the impact stage considering cases with barrier not overtopped (continuous) and trend of other cases (dashed).

The presence of two barriers (Case N5) causes the PRWP value to go up to around 0.3 (Fig. 11). There is hardly any difference among Case N2 and Case N3 and Case N1 (natural slope), indicating that the barrier has little effect on RPWP when Fr > 1 (i.e. supercritical flow) (Fig. 10). On the contrary, RPWP values for Case N5 with Fr < 1 differ remarkably from those for Case N1 (natural slope).

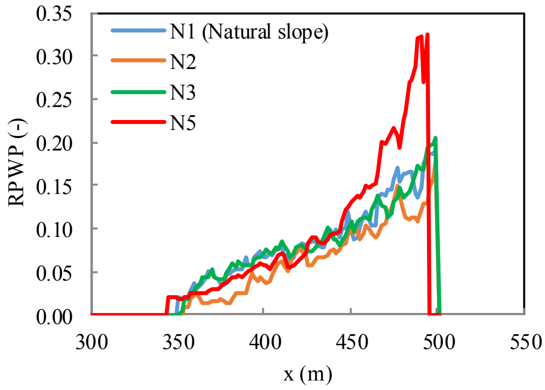

Figure 11. Envelope of pore water pressure along the slope during 20 seconds.

The barrier helps reduce the bed entrainment and this effect is remarkable around 50 m downstream of the barrier. The reduction is evident particularly in case N5 with two barriers. The cumulative erosion thickness reduces by about 0.4 m. For this case, the Froude number immediately behind the first barrier is found to be less than 1.0 and bed entrainment is lower than for the natural slope. On the other hand, the bed entrainment in either Case N2 or N3 with Fr > 1 differ little from that in Case N1 (natural slope), and thus the downstream conditions does not influence the flow features.

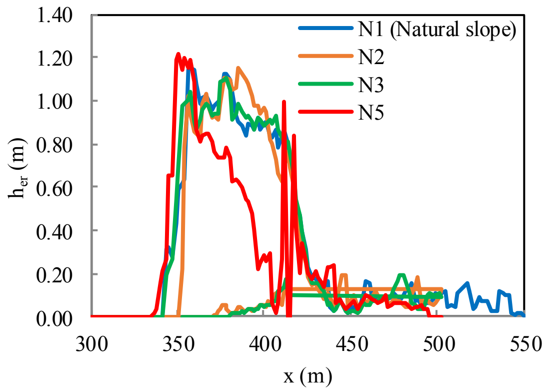

Figure 12. Cumulative erosion thickness along the slope at the final step.

The parameters I_{PRR} and I_{LS} were computed to evaluate the efficiency of the barrier (Fig. 12). In the case of two-barriers (case N5) there is a runout reduction of about 15% (i.e. $I_{PRR} = 0.85$) with the increase of lateral width of about 4%, while for the other cases the reduction is less than 5% with an increase in lateral spreading of about 20%. Thus, the construction of a single barrier would be almost useless for this specific study area. In a combination of two barriers, the first barrier reduces the flow velocity and the second barrier stops the flow. The maximum reduction of runout in presence of two barriers (Case N5) is 15% (Fig. 13). The other cases present low reduction of runout and significant increase of lateral spreading that is higher than 20% compared to the natural slope.

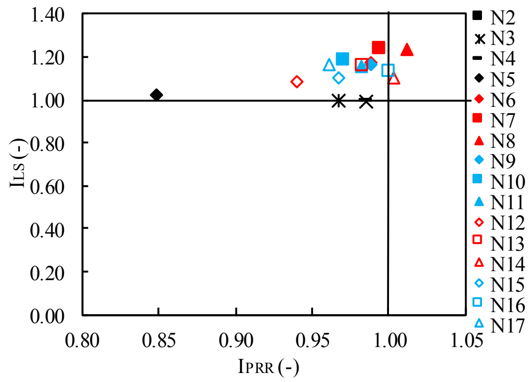

Figure 13. Index of lateral spreading (I_{LS}) and index of piedmont runout reduction (I_{PRR}) computed for the different cases (in black: cases with barrier not overtopped; red: barrier 5 m high; blue: barrier 7 m high).

5 Discussion

The numerical results indicate that the farther the barrier is from the toe of the slope, the smaller is the Froude number of the flow, decreasing from 3 to 1.5. This is important because Fr > 1 indicates that the flow is supercritical and is independent on downstream conditions. RPWP values for the simple topography (Fig. 5b) are about identical to those for the natural slope (Case S10 and Case S11), with Fr > 1 (Fig. 4b). On the other hand, when Fr ≈ or < 1 as shown in Case S8 (x = 255 m), RPWP values are influenced by the barriers (Fig. 5a). Similar considerations can be given to the case study of Nocera Inferiore. For instance, Case N2 and Case N3 with Fr > 1 (Fig. 10), RPWP values are about identical to those for the natural slope N1 (Fig. 11); while, Case N5 (x = 435 m) with Fr < 1, RPWP values differ from those in Case N1. Thus, the type and location of the barrier should decrease the Froude number of the flow until deposition.

We compared the results for the simple topography and case study in terms of I_{PRR} and I_{LS} (Fig. 14). The barrier in the simple topography cases decreases the runout significantly in comparison to the real topography case. At the same time, lateral spreading of the flowing slurry is more significant in real topography than in the simple topography. In real topography, the flow is first partially channelized, and then accelerated. The barrier effect on runout is less significant with the reduction of about 5%. Furthermore, there is a higher increase of I_{LS} in the real topography than the simple topography case, being > 30% and < 10%, respectively.

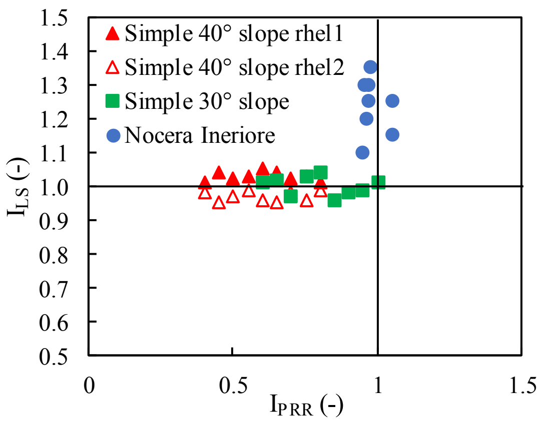

Figure 14. Comparison between several results in terms of index of lateral spreading (I_{LS}) and index of piedmont runout reduction (I_{PRR}) computed for the different cases.

6 Conclusions

The effects of artificial barriers on the features of debris avalanches were analysed via numerical modelling. A quasi-3D SPH hydro-mechanically coupled model was used to simulate the propagation heights and velocities, the evolution of pore water pressures inside the flow and the entrainment of additional material from the ground surface during the propagation stage. The numerical simulations focused on schematic open slopes resembling typical in-situ conditions and on the study area of Nocera Inferiore (Southern Italy) where a destructive debris avalanche occurred in 2005. Different scenarios were analysed relative to the number, type and location of the artificial barriers.

In order to compare the different cases, we newly defined two parameters to evaluate the efficiency of one or two barriers. The indexes I_{PRR} and I_{LS} represent the reduction in runout and the increase in lateral width caused by the barriers once a comparison is made with the natural slope.

The numerical results highlighted the differences in propagation pattern, velocity and deposition thickness of the flows in presence of artificial barriers. Generally, runout decreased down to 70% when the barrier was very close to the toe of the slope (Case S3), while the landslide runout slightly increased (but with lower thickness) when the barrier was positioned along the 35° steep piedmont slope compared to natural slope (Case N8). The highest efficiency of the barrier was obtained when the barrier was located immediately at the toe of the slope or at a few meters distance or even in presence of two barriers. Furthermore, the barrier type differently influenced the area affected by the flow passing from Type I to Type II barriers positioned at the same distance from the source area. In particular, I_{PRR} decreased with Type II compared to Type I, when the barrier was nearer to the source area. It can also be noted that for the barrier farthest from the source area, I_{PRR} did not change significantly passing from Type I to Type II.

The barriers may change the features of the propagating flows (height, velocity, lateral width, and extent of the material) and their tempo-spatial distribution. Both height and width of the flow increased behind the barrier if not overtopped.

In conclusion, this paper analysed the effects of artificial barriers on the change in the features of flow-like landslides, considering the role of type and location of the barriers, the reduction of runout, the changes in involved area, velocity, deposition height, and duration of the impact stage. Such research should be extended to other flow rheologies and slope geometries. In particular, accurate analyses could be necessary in case of partially channelized flow due to local topography. Another improvement could come from the use of fully-3D modelling which could enhance the accuracy of the numerical analysis, especially for the smallest sizes of the barrier considered in this paper.

Acknowledgements

This research was developed within the framework of different projects: i) Industrial Partnership PhD Course (Dottorato Industriale Regione Campania, Italia); ii) project FARB 2017 "Modellazione numerica e analisi inversa per frane tipo flusso" funded by the Italian Education and Research Ministry. Prof. Manuel Pastor (Universidad Politecnica de Madrid, Spain) and co-workers are much acknowledged for having provided the "GeoFlow_SPH" code used for the numerical simulations. We are grateful to Dr. Anika Braun (TU Berlin) for English proofreading.

7 References

Armanini A, Larcher, M, & Odorizzi, M (2011) Dynamic impact of a debris flow front against a vertical wall. In Proceedings of the 5th International Conference on Debris-Flow Hazards Mitigation: Mechanics, Prediction and Assessment, Padua, Italy, 1041-1049.

Brandl H (2011) Geosynthetics applications for the mitigation of natural disasters and for environmental protection. Geosynthetics International, 18(6):340-39 0.

Blanc T (2008) Numerical simulation of debris flows with the 2D-SPH depth integrated model. Master thesis. UPM, Spain.

Braun, A., Cuomo, S., Petrosino, S., Wang, X., Zhang, L. (2018). Numerical SPH analysis of debris flow run-out and related river damming scenarios for a local case study in SW China. Landslides, 15(3), 535-550.

Bugnion L, McArdell BW, Bartelt P, & Wendeler C (2012) Measurements of hillslope debris flow impact pressure on obstacles. Landslides, 9(2):179-187.

Calvetti F, di Prisco CG, Vairaktaris E (2017) DEM assessment of impact forces of dry granular masses on rigid barriers. Acta Geotechnica, 12(1):129-144.

Canelli L, Ferrero AM, Migliazza M, Segalini A (2012) Debris flow risk mitigation by the means of rigid and flexible barriers-experimental tests and impact analysis. Natural Hazards and Earth System Sciences, 12(5), 1693.

Cascini L, Cuomo S, Della Sala M (2011a) Spatial and temporal occurrence of rainfall-induced shallow landslides of flow type: A case of Sarno-Quindici, Italy. Geomorphology, 126(1-2), 148-

158.

Cascini L, Cuomo S, De Santis A (2011b) Numerical modelling of the December 1999 Cervinara flow-like mass movements (Southern Italy). Proc. of 5th International Conference on Debris-Flow Hazards Mitigation: Mechanics, Prediction and Assessment. Italian Journal of Engineering Geology and Environment, 635-644.

Cascini L, Cuomo S, Pastor M, Sorbino G, Piciullo L (2014) SPH run-out modelling of channelised landslides of the flow type. Geomorphology, 214, 502-513.

Cascini L, Cuomo S, Pastor M, Rendina I (2016) SPH-FDM propagation and pore water pressure modelling for debris flows in flume tests. Engineering Geology, 213, 74-83.

Cascini S, Cuomo S, Pastor M, Rendina, I (2018) Modelling of debris flows and flash floods propagation in storage basins of Italian Alps. Landslides (under review).

Ceccato F, Simonini P, di Prisco C, Redaelli I (2017) The effect of the front inclination on the impact forces transmitted by granular flows to rigid structures. In Workshop on World Landslide Forum, 593-599. Springer, Cham.

Choi CE, Law RP (2015) Performance of landslide debris-resisting baffles. HKIE Transactions, 22(4), 235-246.

Choi CE, Ng CWW, Au-Yeung SCH, Goodwin GR (2015) Froude characteristics of both dense granular and water flows in flume modelling. Landslides, 12(6):1197-1206.

Cuomo S, Pastor M, Cascini L, Castorino GC (2014) Interplay of rheology and entrainment in debris avalanches: a numerical study. Canadian Geotechnical Journal, 51(11), 1318-1330.

Cuomo S, Pastor M, Capobianco V, Cascini L (2016) Modelling the space–time evolution of bed entrainment for flow-like landslides. Engineering Geology, 212, 10-20.Cuomo S, Cascini L, Pastor M, Petrosino S. (2017) Modelling the propagation of debris avalanches in presence of obstacles. In Workshop on World Landslide Forum (pp. 469-475). Springer, Cham.

Ferrari A, Dumbser M, Toro EF, Armanini A. (2009) A new 3D parallel SPH scheme for free surface flows. Computers & Fluids, 38(6), 1203-1217.

Hungr O, Evans SG, Bovis MJ, Hutchinson JN (2001) A review of the classification of landslides of the flow type. Environmental & Engineering Geoscience, 7(3), 221-238.

Leonardi A, Wittel FK, Mendoza M, Vetter R, Herrmann HJ (2016) Particle–fluid–structure interaction for debris flow impact on flexible barriers. Computer-Aided Civil and Infrastructure Engineering, 31(5), 323-333.

Kattel P, Kafle J, Fischer JT, Mergili M, Tuladhar BM, Pudasaini SP (2018) Interaction of two-phase debris flow with obstacles. Engineering Geology.

Kwan JSH, Koo RCH, Ng CWW (2015) Landslide mobility analysis for design of multiple debris-resisting barriers. Canadian Geotechnical Journal, 52(9), 1345-1359.

Mizuyama, T (2008) Structural countermeasures for debris flow disasters. International Journal of Erosion Control Engineering, 1(2), 38-43.

Monaghan JJ(1994) Simulating free surface flows with SPH. Journal of computational physics, 110(2), 399-406.
Ng CWW, Choi CE, Song D et al. (2015) Physical modeling of baffles influence on landslide debris mobility. Landslides 12(1): 1-18.
Popescu ME, Sasahara K (2009) Engineering measures for landslide disaster mitigation. Landslides–Disaster Risk Reduction, 609-631.
Pastor M, Haddad B, Sorbino G, Cuomo S, Drempetic V (2009) A depth-integrated, coupled SPH model for flow-like landslides and related phenomena. International Journal for numerical and analytical methods in geomechanics, 33(2), 143-172.
Revellino P, Guadagno FM, Hungr O (2006) Criteri morfologici e modellazione dinamica nella valutazione della suscettibilità da frana lungo versanti carbonatici dell'Appennino Campano. Giornale di Geologia Applicata, 3, 159-166.
Ronco C, Oggeri C, Peila D (2009) Design of reinforced ground embankments used for rockfall protection. Natural Hazards and Earth System Sciences, 9(4), 1189-1199.
Wendeler C, Volkwein A, Denk M, Roth A, Wartmann S (2007) Field measurements used for numerical modelling of flexible debris flow barriers. In: CL Chen, JJ Major (eds). Proceedings of Fourth International Conference on Debris Flow Hazards Mitigation: Mechanics, Prediction, and Assessment, 10-13 September 2007. Chengdu, China. pp. 681–687.